Medical Engineering and Physics 65 (2019) 31–38

Contents lists available at ScienceDirect

Medical Engineering and Physics

journal homepage: www.elsevier.com/locate/medengphy

# Determination of local micromotion at the stem-neck taper junction of a bi-modular total hip prosthesis design

Adrian Falkenberg*, Paul Drummen, Michael M. Morlock, Gerd Huber

*Institute of Biomechanics, Hamburg University of Technology (TUHH), Denickestrasse 15, Hamburg 21073, Germany*

ARTICLE INFO

*Article history:*
Received 6 August 2018
Revised 8 January 2019
Accepted 10 January 2019

*Keywords:*
Bi-modular prosthesis
Taper junction
Micromotion
Assembly force
Flexural rigidity

ABSTRACT

High rates of clinical complications with bi-modular hip prostheses are attributed to failure of the stem-neck taper junction. Taper wear analyses have shown extensive material loss as a result of corrosion, potentially initiated by micromotion. The purpose of the study was to determine the amount of micromotion at this junction for different loading, assembly and material conditions.

Micromotion between the neck adapter (CoCr29Mo6-alloy) and the stem (TiMo12Zr6Fe2-alloy; both Rejuvenate, Stryker) within the taper junction of a bi-modular hip stem were determined by image matching analysis of consecutively recorded images through windows in the stem component. A finite element model was used to determine the micromotion in the taper regions outside the windows and validated with the measured micromotion. With the model, the influence of the load amplitude, assembly force and component materials were then investigated. Determined micromotion (14–79 µm) by far exceeded critical values (5 µm) associated with the onset of fretting corrosion. Increasing assembly forces achieved a significant reduction in micromotion. The numerical model revealed insufficient assembly to cause the neck to perform rocking motions under load, repetitively changing taper contact in combination with gap opening, which facilitates fluid ingress into the junction. Changing the stem material to a stiffer Ti-alloy achieved a reduction of the micromotion of about 30%. This study emphasises the high importance of material selection, assembly force and loading on the susceptibility of bi-modular hip stems to fretting and crevice corrosion. These findings can serve to explain the increased rate of clinically reported problems with this particular prosthesis design.



## 1. Introduction

Numerous retrieval studies have documented clinical failure of modular total hip arthroplasties following corrosion and material loss [1,–3]. Metal debris from corroding taper junctions released into the periprosthetic tissue of the patient's body leads to elevated serum metal ion levels. These can potentially trigger various symptoms including pseudo-tumour formation [4,5], osteolysis [6] or substantial soft-tissue necrosis [7], causing severe pain followed by implant instability and therefore requiring revision surgery.

More incidents of corrosion related failure have been reported for bi-modular prostheses, reflected by twice as high revision rates compared with fixed neck prostheses [8]. Clinical follow-ups showed devastating implant survivorships of 30% after three years [9] and 14% after four years [10] for one specific prosthesis design. The taper junction connecting stem and modular neck appears to be the susceptible link, exhibiting excessive corrosion and material loss [11]. Retrieval studies found fretting and corrosion at the stem-neck interface in every analyzed prosthesis [12]. Implants with long neck lengths showed significantly higher corrosion scores and younger patient age concomitant with higher daily activity were highlighted as potential factors for early failure [13].

Various interpretations have been proposed for implant failure caused by taper corrosion and clinical evidence is strongly indicative of a multifactorial cause [14–17]. However, a prerequisite for the onset of fretting corrosion appears to be micromotion between the mating surfaces of a taper junction [12]. Micromotion initiates local abrasion of the metals' oxide film and continuous re-passivation lowers the pH of surrounding fluid, developing an acidic solution that progressively attacks the metal surface. Previously, micromotions within the junction were either determined based on numerical modeling [18] or indirectly measured by external fixtures via contactless relative motion measurement techniques [19,20]. The former is limited due to the limited knowledge concerning friction parameters in the junction in-situ and the lack of appropriate validation measurements, while the latter method is limited in distinguishing between local micromotions in the

* Corresponding author.
*E-mail address:* adrian.falkenberg@tuhh.de (A. Falkenberg).

https://doi.org/10.1016/j.medengphy.2019.01.003
1350-4533/

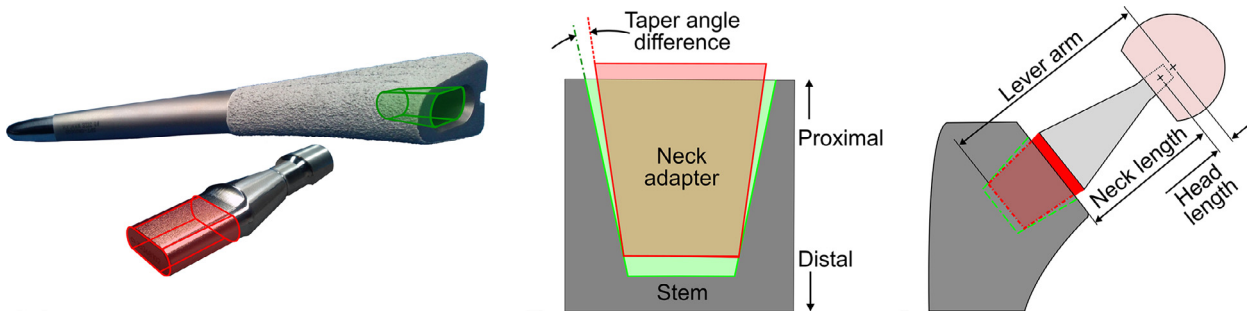


**Fig. 1.** Stem and neck adapter of the bi-modular prosthesis investigated (A). The male neck taper is highlighted in red and the female stem taper in green. Distal taper engagement occurred due to a positive taper angle difference (B). The lever arm between head centre and taper engagement is given by the combination of neck length and head offset (C).

**Table 1**
Technical data of the prostheses used and time in-situ (see Fig. 1 for explanations of parameters).

| Prosthesis | Taper angle difference [°] | Lever arm [mm] | Neck width min. / max. [mm] | Neck length [mm] | Head length [mm] | Head diameter [mm] | Time in-situ [mths] |
|---|---|---|---|---|---|---|---|
| *High* | 0.028 | 60 | 13.0 / 18.4 | 42 | −4 | 36 | 35.7 |
| *Low* | 0.053 | 60 | 12.8 / 17.5 | 38 | 0 | 40 | 38.1 |

junction and elastic deformations of the surrounding implant, which artificially increase the measured relative movement of the externally mounted sensors.

The aim of this study was to determine locally occurring micromotion within the taper junction of a bi-modular total hip prosthesis using an experimental approach and to determine how assembly force, loading and the use of other materials influences the micromotion based on numerical simulation.

## 2. Material and methods

The micromotion behavior at the flat taper junction (Fig. 1) between a modular neck adapter (CoCr29Mo6-alloy, referred to as CoCr) and stem (TiMo12Zr6Fe2-alloy, referred to as TMZF) of a bi-modular prosthesis design (Rejuvenate, Stryker Orthopaedics, Mahwah, New Jersey) was assessed in a combined approach of experimental in-vitro testing and numerical simulation.

### 2.1. Experimental testing

Two retrieved prostheses from one patient (bi-lateral, 52 years, male, 90.7 kg, 27.1 BMI) with marginally worn taper surfaces and similar stem sizes (size 9, 142 mm) were used for the measurements (Table 1). In an earlier study, detailed taper parameters for these retrievals were determined based on tactile measurements (BHN 805, Mitutoyo, Tokyo, Japan) and best fit approximation [11]. The stems were truncated according to ISO 7206-4 for mounting purposes.

The lever arm between head centre and taper engagement of the assembled prostheses were similar, despite the varying neck geometries with respect to width and length, since the differences were compensated by different head lengths (Table 1). The flexural stiffnesses, however, were different. These are referred to as '*High*' (broad neck, short head) and '*Low*' (narrow neck, long head). The positive values for the taper angle difference (Table 1) indicate that both prostheses had a distal taper engagement mainly at the apex of the hemi-circular cross section (Fig. 1) [21].

The micromotion of the male taper surface of the neck adapter with respect to the female taper surface of the stem was directly measured through two windows (Fig. 2). The windows were eroded through the stem by electric discharge machining (AgieCharmilles FORM 20, GF Machining Solutions GmbH, Losone, Switzerland). Utilizing this method burr-free cavities were created, which averted unintended surface damage to the neck adapter during assembly with the stem. The windows were designed as truncated pyramids with an angle resembling the microscope's angle of view, therefore achieving proper light guidance and adequate illumination of the surfaces of interest. The windows had an edge length of 1.5 mm at the narrow end to keep the influence on the structure's integrity negligible. Load transfer in this type of junction is mainly provided through the contact at the apexes [21]. Therefore, the windows were positioned close to the proximal and distal end of the flat taper junction, where taper contact is not expected (Fig. 2). This kept the interfacial stress distribution inviolate, which was checked by finite element analysis (results not shown). Distance from the windows' centres to the edges of theoretical taper engagement was 8 mm and 2 mm for the proximal and distal window, respectively.

The original ceramic ball heads, neck adapters and stems were quasi-statically assembled under 2000 N using an uniaxial material testing machine (Z010, Zwick Roell AG, Ulm, Germany), which corresponds to intraoperative forces at the femur, rather than the impaction device. Afterwards, the prosthesis was rigidly mounted in a load rig (Fig. 2) for micromotion measurements. Loads were applied to the ball head via a screw thread and measured by a force sensor in-between head and screw thread. The axis of the stem was aligned with the direction of load application, creating an in-plain static load case. Quasi-static mechanical testing included preconditioning and three loading sequences. Preconditioning (1900 N) was performed to accommodate eventual further seating of the neck in order to avoid superposition of micromotion with seating motions. Each loading sequence covered three consecutively applied load steps of 1000 N, 1500 N and 1900 N, with the highest load corresponding to hip forces during walking [22]. After each loading sequence, the prosthesis was unloaded. The procedure was then repeated with 4000 N assembly force.

The male taper surface visible through the window was recorded using focus stacked 2D topographical images (Infinite Focus Microscope G4, Alicona Imaging GmbH, Graz, Austria) with an in plane resolution of 1.75 µm and a topological resolution of 0.30 µm. The load rig was placed under the microscope after each load application, which inevitably caused slight deviations in the position of the prosthesis with regard to the microscope's coordinate system (Fig. 3(B)). In order to align the different

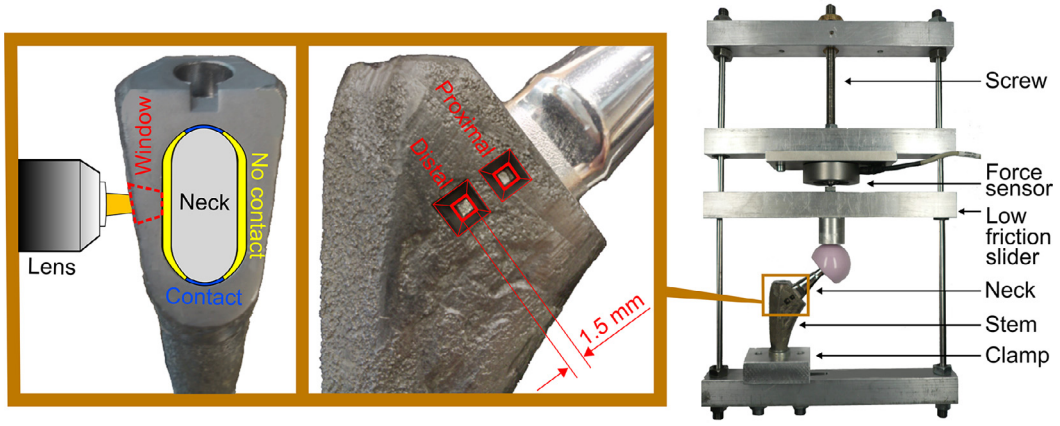


**Fig. 2.** Left; Setup for micromotion measurements with the stem prepared with windows shaped as truncated pyramids in regions of no taper contact at the proximal and distal end of the flat taper junction. Right. The truncated prosthesis mounted to the load rig for static force application via a screw thread at the top.

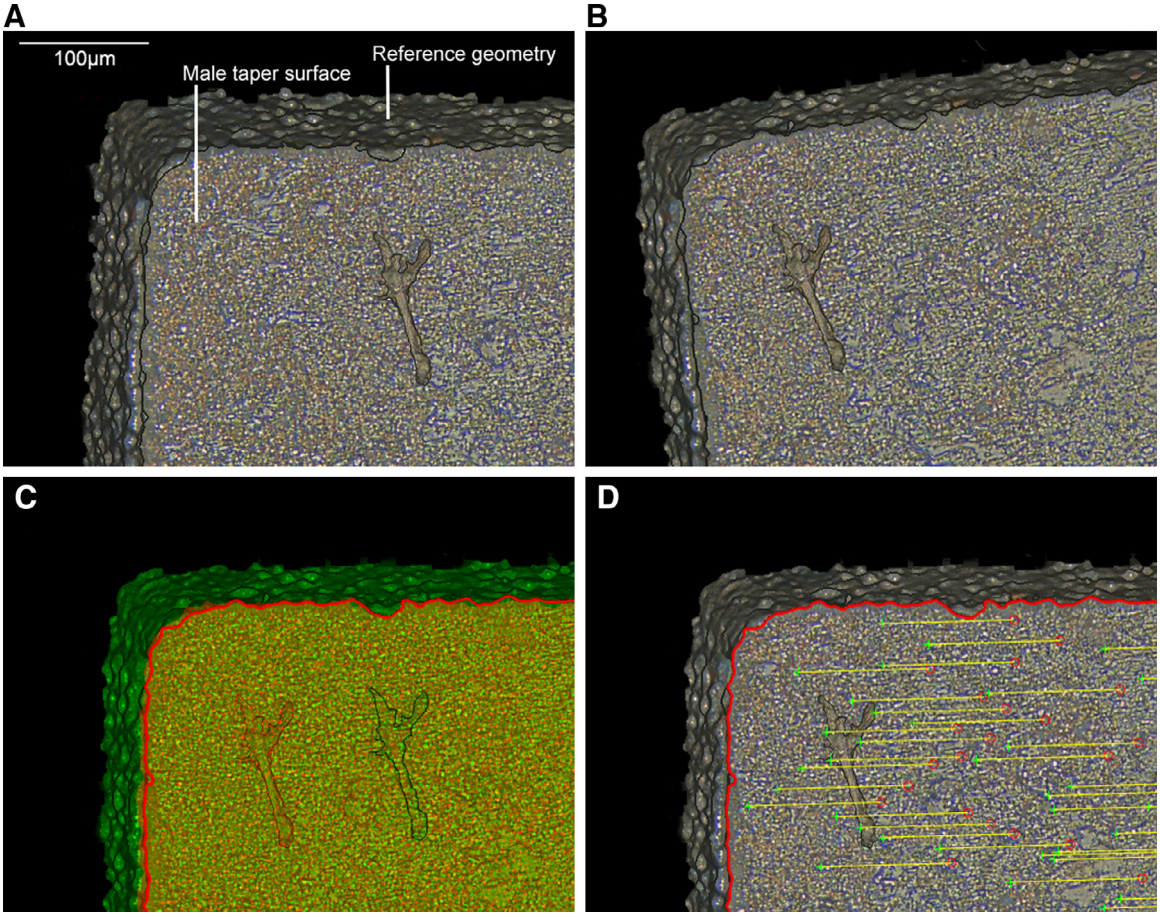


**Fig. 3.** Focus stacked 2D images from topographic microscopic measurements to compute interfacial micromotion. (A) Microscopic exposure of the male taper surface and the female taper's wall as reference geometry at Time i. (B) After load application, micromotion at the taper junction and a rotation of the image of Time i + 1 due to rearranging the load rig after load application. (C) Segmentation of the male taper surface from the female taper to obtain reference boundaries (red line). Calculation of the transformation matrix by aligning the boundary lines, and its application to the position at Time i + 1. (D) Image matching for computation of interfacial micromotion. The red circles represent the initial positions of the points selected by the matching algorithm; the green crosses represent the end position. The yellow lines show the magnitude and direction of micromotion.

measurements, a part of the window wall in the stem was captured together with the male taper surface of the neck adapter (Fig. 3(A)). The topography of the male taper surface was analyzed with respect to the reference geometry of the window wall. The image processing included the segmentation of the male taper surface with respect to the adjacent female taper for the images of the prosthesis in its current loading state (Time i) and its consecutive loading state (Time i + 1) obtaining the interfacial boundaries. The boundary lines of subsequent images were then used to calculate the rigid body transformation between Time i and Time i + 1. In a following step, this transformation was applied to the segmented male taper surface of Time i + 1, thus yielding its projection into the position at Time i, solely differentiated by the relative motion of the male taper in-between the respective subsequent loading

states (Fig. 3(C)). In the final step, the interfacial micromotion was calculated by image matching algorithms (Matlab 2015a, The MathWorks Inc., Natick, USA), (Fig. 3(D)). Pilot studies with simplified components subjected to predefined relative motions were performed. A plate prepared with a window equivalent to the windows in the stems was moved on a fixed ground in the microscope's global coordinate system. This displacement was compared to the micromotion calculated from the developed method based on consecutive images in their local coordinate systems, which exhibited an accuracy of 0.1 µm.

Three general comparisons were made. First, micromotion was determined for every pair of consecutive load steps to exhibit the influence of load increase. Second, additional seating as a result of loading was determined by comparison of the states of 0 N from before and after a loading sequence. Third, the initial positions after assembly with 2000 N and 4000 N were compared to determine the difference in seating depth of the neck adapter.

Statistical analyses of the former two comparisons were performed using t-tests with a type I error probability of $\alpha = 0.05$ (SPSS Statistics 23, IBM Corporation, Armonk, USA). Measurements from the two different prostheses were regarded as two separate groups.

### 2.2. Numerical analysis

To determine the micromotion at regions that could not be observed experimentally, a finite element (FE) model (Abaqus/Standard 6.14, Dassault Systemes, Vélizy-Villacoublay, France) of the test set-up based on prosthesis *High* was created (Fig. 6). The geometry of the stem was captured by 3D laser scanning (50 µm resolution, HandyScan 3D, Creaform, Quebec, Canada). Prosthesis specific taper parameters obtained from tactile coordinate measurements [11] were used for the modeling of the male and female taper surfaces. Linear elastic and homogeneous material properties (Young's modulus, Poisson's ratio) were assigned to the stem (76 GPa, 0.33) and the neck (221 GPa, 0.30) component. The electrically discharged windows were neglected in the model.

In the simulations all translational degrees of freedom were fixed at the bottom of the stem. Forces were applied to a reference point at the approximated location of the head centre. The stem and neck were discretized with quadratic tetrahedron elements, whereas the female and male taper geometries were partitioned and meshed separately with hexahedrons utilizing linear Ansatz-functions. A penalty contact formulation was chosen (coefficient of friction $\mu = 0.3$, [23]); the neck was assigned the master surface due to its higher stiffness. In the proximity of taper engagement high stress gradients were anticipated, consequently inducing mesh refinements. Detailed mesh convergence studies were carried out with regard to von Mises stress, contact stress as well as contact penetration into the slave surface. An element edge length of 0.125 mm was deemed valid for the female taper area; the global element size was set to 2 mm.

The micromotion calculation was divided into several steps. From the FE result file, the node coordinates of the taper surfaces were extracted via a Python-script and imported in Matlab for further investigation. First, for every node on the male taper surface the closest node on the female taper surface was determined to obtain node pairs. For those node pairs, the individual relative displacements were calculated in every load step. Finally, the difference of relative displacements in between the load steps was the measure for micromotion. Model validation was performed against the experimentally measured micromotion in the theoretical window areas.

The FE model was used to calculate micromotions for assembly forces of 2000 N, 4000 N and 8000 N, for joint load amplitudes of 1900 N (walking) and 4300 N (climbing stairs), for in-vivo load direction (10° adduction and 9° flexion), as well as for a stem made from contemporary Ti6Al4V (110 GPa, 0.34). Furthermore, lateral gap opening of the taper junction under load was investigated.

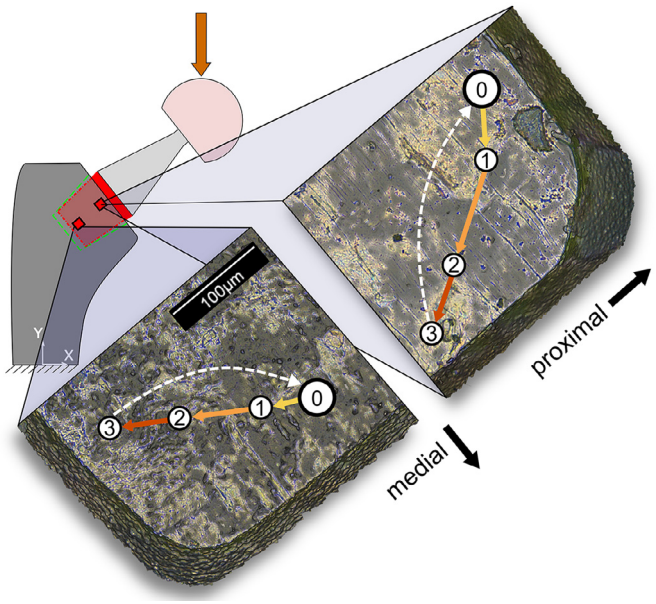


**Fig. 4.** Motion pattern of the neck under load observed through the proximal and distal window in either prosthesis after assembly of 2000 N (left). Starting from zero loading (0); the locations 1, 2 and 3 are relative movements after the respective load steps. The dotted white arrow indicates the return of the neck into its initial position upon unloading. The scale is related to the surface while the motion (arbitrary point on the male taper surface) is magnified by 20-times.

## 3. Results

### 3.1. Experimental testing

A similar distinct motion pattern during loading was observed for both prostheses for the lower assembly force (Fig. 4). The motion was composed of a component pointing in the taper axis direction, pushing the neck adapter deeper into the stem, which was superimposed by a component transversal to it, resulting in simultaneous rocking. At the proximal window, the transversal component pointed in medial direction, whereas at the distal window the neck moved towards lateral, suggesting an instantaneous point of rotation at the prosthesis' lateral side between the two windows. With the higher assembly force, the motion pointed mainly towards medial rather than in axial direction at the proximal window, similar to the motion illustrated in Fig. 4 from location 0 to location 1.

Micromotion between the stem and neck adapter increased with loading and decreased with increasing assembly force and prosthesis stiffness (Fig. 5). For prosthesis *High* assembled with 2000 N, a loading of 1000 N caused micromotion of $2.9 \pm 1.1$ µm and $2.6 \pm 0.5$ µm at the proximal and distal window, respectively. Load increase to 1500 N yielded additional micromotion of $4.4 \pm 0.7$ µm and $4.2 \pm 0.8$ µm. In the last load step of 1900 N additional micromotions of $4.1 \pm 0.5$ µm and $4.0 \pm 0.7$ µm were measured, accumulating the total micromotion to $11.4 \pm 1.1$ µm in the proximal and $10.8 \pm 0.2$ µm in the distal window (Fig. 5, Table 2). The amount of micromotion at the proximal and distal window was equal for either prosthesis ($p = 0.423$, Table 2). Prosthesis *Low* showed significantly higher total micromotions than prosthesis *High* at the proximal ($14.2 \pm 1.0$ µm, $p = 0.032$) and at the distal window ($14.2 \pm 1.9$ µm, $p = 0.038$, Fig. 5).

**Table 2**
Micromotion measured at the proximal and distal windows in loading sequence 1 / 2 / 3 for prostheses *High* and *Low* after assembly with 2000 N.

| Micromotion [µm] | | Load step | | | |
|---|---|---|---|---|---|
| | | 0–1000 N | 1000–1500 N | 1500–1900 N | Total |
| *High* | Proximal | 1.7 / 3.2 / 3.8 | 3.7 / 5.1 / 4.3 | 4.7 / 3.7 / 4.0 | 10.1 / 12.0 / 12.1 |
| | Distal | 2.4 / 2.3 / 3.2 | 3.7 / 5.1 / 3.9 | 4.8 / 3.6 / 3.5 | 10.9 / 11.0 / 10.6 |
| *Low* | Proximal | 3.2 / 4.5 / 3.3 | 8.1 / 5.9 / 7.0 | 3.2 / 4.6 / 2.8 | 14.5 / 15.0 / 13.1 |
| | Distal | 2.9 / 2.2 / 2.5 | 8.4 / 7.0 / 8.4 | 4.8 / 3.2 / 3.4 | 16.1 / 12.4 / 14.3 |

**Table 3**
Micromotion measured at the proximal and distal windows in loading sequence 1 / 2 / 3 for prostheses *High* and *Low* after assembly with 4000 N.

| Micromotion [µm] | | Load step | | | |
|---|---|---|---|---|---|
| | | 0–1000 N | 1000–1500 N | 1500–1900 N | Total |
| *High* | Proximal | 1.1 / 1.0 / 1.0 | 0.9 / 1.3 / 2.2 | 2.7 / 2.0 / 2.5 | 4.7 / 4.3 / 5.7 |
| | Distal | 0.7 / 0.2 / 0.8 | 0.9 / 0.5 / 1.2 | 2.9 / 2.9 / 2.6 | 4.5 / 3.6 / 4.6 |
| *Low* | Proximal | 1.6 / 0.5 / 0.4 | 1.2 / 0.9 / 1.0 | 2.1 / 2.0 / 1.7 | 4.9 / 3.4 / 3.1 |
| | Distal | 1.2 / 0.5 / 0.5 | 1.9 / 0.4 / 0.3 | 1.9 / 2.1 / 1.5 | 5.0 / 3.0 / 2.3 |

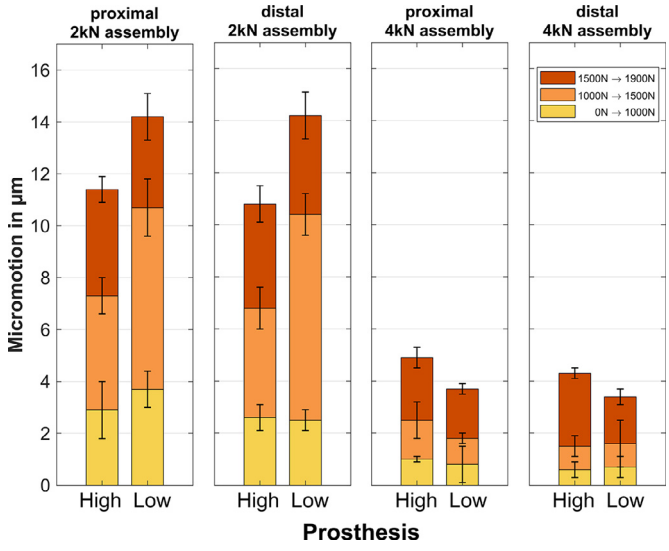


**Fig. 5.** Experimentally measured micromotion at the proximal and distal windows for prostheses *High* and *Low* for the two different assembly forces.

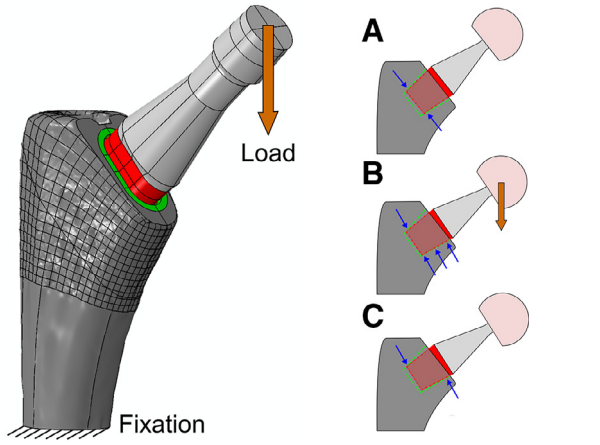


**Fig. 6.** Left. Finite element model of prosthesis *High* generated from a 3 D scan of the stem and tactile measurements of the male and female taper surfaces. Right. Taper contact conditions; (A) Initial distal taper engagement after assembly (blue arrows). (B) Contact along the medial face during loading. (C) Permanent neck tilt after loading.

Secondary seating (difference between the unloaded state before and after preconditioning) for assembly with 2000 N was 2.0 µm and 2.5 µm for prostheses *High* and *Low*, respectively. Nearly no further seating during the following loading sequence was observed (less than 0.5 µm).

Measurements with an assembly force of 4000 N exhibited significantly less micromotion ($p<0.001$) compared to the assembly force of 2000 N (Fig. 5, Table 3) with no differences between the prostheses ($p=0.189$).

Comparison of the initial unloaded states after assembly with 2000 N and 4000 N showed differences in seating depths. For the assembly with 4000 N, the neck adapter of prosthesis *High* travelled 78 µm deeper into the stem compared with the 2000 N assembly (prosthesis *Low*: 118 µm). This displacement was observed through both windows.

### 3.2. Numerical analysis

The calculated micromotion in the window areas was similar to the results of the experimental testing regarding quantity as well as quality in terms of the observed motion patterns. Loading with 1000 N/1500 N/1900 N (after 2000 N assembly) yielded micromotion of 1.9/4.0/5.4 µm in the region of the proximal and 1.6/3.4/5.0 µm in the region of the distal window. In total, the micromotion accumulated to 11.3 µm proximally and 10.1 µm distally. For validation purposes, these values were compared to the experimentally measured values (11.4 ± 1.1 µm and 10.8 ± 0.2 µm, respectively, Table 2). This deviation was less than 10%.

For the assembly with 2000 N, a permanent alteration in contact condition upon first loading was observed. The initial distal taper engagement after assembly (Fig. 6(A)) changed to contact of the neck with the female taper along the medial face during loading (Fig. 6(B)). Removal of the load exhibited a permanent neck tilt with diagonal contact from lateral-distal to medial-proximal (Fig. 6(C)), which was more pronounced for high loads (4300 N). Subsequent cyclic loading resulted in a rocking motion of the neck around an almost fixed point at the lateral-distal site, repetitively opening a gap at the lateral-proximal taper end. For the 1900 N load, a gap of 19 µm between the male and female taper surface, as well as high micromotion of up to 20 µm along the medial face was observed (Fig. 7(A)). The highest load (4300 N) increased gap opening to 46 µm and micromotion to 79 µm (Fig. 8).

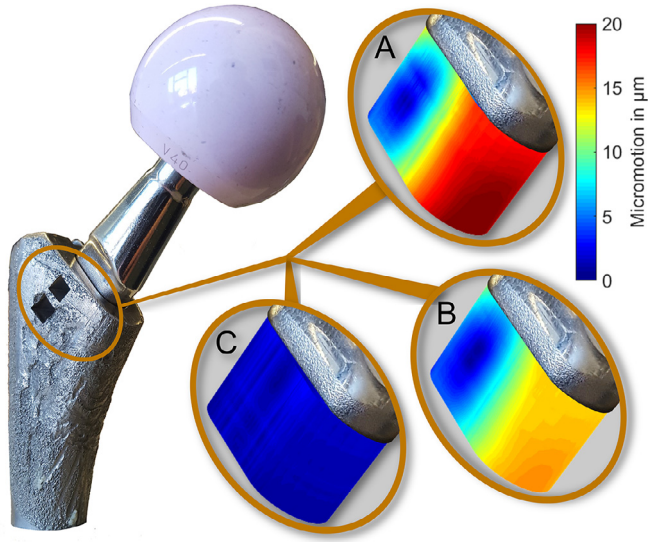


**Fig. 7.** Results of the FE simulation for the locally occurring micromotion between the neck adapter and stem. (A) Micromotion exceeding 20 µm was determined at the medial taper contact under loads of 1900 N for Prosthesis *High*. (B) Reduced micromotion under the same loading condition in case of Ti6Al4V as stem material. (C) Micromotion reduction achieved by applying higher assembly forces (8000 N).

Compared to assembly with 2000 N, increasing the assembly force to 4000 N showed reductions in micromotion of 40% (medial), a further increase to 8000 N yielded an additional decrease of 70% (Fig. 7(C)). Assembly forces of 4000 N and higher also prevented a permanent neck tilt under moderate loads. Gap opening was reduced to 8 µm for walking (1900 N) after assembly with 8000 N. Higher load (4300 N) resulted in micromotion of 18 µm and a permanent neck tilt. The in-vivo load cases showed a slight shift of the medial and lateral contact area towards the direction of the load and caused partial contact at the flat taper regions (posterior), while micromotion magnitudes and gap opening remained similar.

Using conventional Ti6Al4V as stem material reduced the micromotion at the taper junction for all load conditions, most notably (30% reduction) for the 2000 N assembly cases (Fig. 7(B)) and for high load amplitudes (Fig. 8). The lateral gap opening during maximum load was also lower (25%). Motion patterns were similar as seen for TMZF and a permanent neck tilt under high loads (stair climbing) was also observed.

## 4. Discussion

Tribological as well as electrochemical aspects were shown to induce a variety of corrosive effects at taper interfaces of modular total hip prostheses in combination with mechanical loading. In this study, the focus was set on the micromotion between the mating surfaces of the taper junction, which is a prerequisite for the onset of fretting and fretting corrosion, which can accelerate into crevice corrosion [14,15,17].

Direct micromotion measurements based on image analysis as well as FE simulations revealed recurring micromotions of the neck adapter under repeated loading. Hence, during any physical activity certain areas - mainly medial-proximal - are repetitively shifting between contact and no contact, which may cause taper surface damage over time. The windows at the proximal and distal taper end enabled predictions of the overall neck motion within the taper junction and gave indication of a rocking motion during loading. Similar rocking-like motions have been observed at the head-stem interface for heads with large offsets and were shown to cause high rates of wear and corrosion [24]. Activities of daily living may exhibit substantially higher amounts of micromotion as seen in the present study, since certain loads during in-vivo

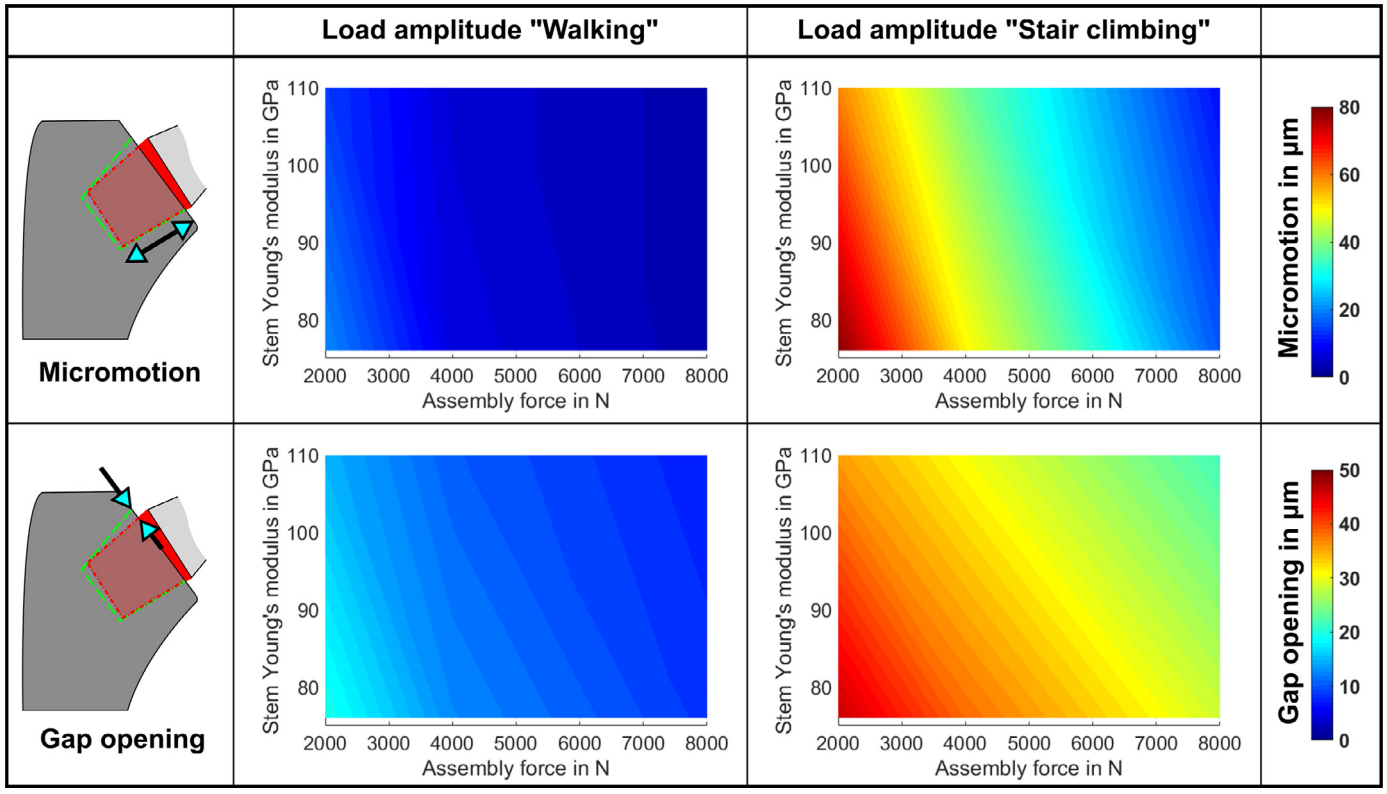


**Fig. 8.** Micromotion along the medial taper face and lateral gap opening for different load amplitudes in combination with assembly forces and stem material as calculated from finite element analyses.

activities exceed the loads experimentally tested in this study [22]. This was confirmed by the FE-model results in this study. Additionally, inadequately lubricated bearings or large heads might even increase micromotions due to high friction moments acting at the articulation surface, which have to be transmitted through the taper junction [25].

A localized distal taper engagement due to a taper angle difference, concentrated predominantly at the taper apexes, is the geometrical prerequisite for the effect observed in this prosthesis. Load transmission through modular hip stems in-vivo without micromotion is unlikely, especially if loads out of plane are applied [21]. The neck constitutes a lever arm, generating high bending moments that the taper-lock has to endure. It was shown that even load magnitudes below the assembly forces can lead to high micromotion within the flat taper junction. Compared with the head-stem taper junction of traditional hip prosthesis stems, the distance between load introduction and taper engagement is longer by a factor of up to 20, which raises concerns over the general mechanical integrity of bi-modular prostheses. Micromotion in this study was significantly influenced by the flexural rigidity of the system as a combination of neck geometry and head length. The use of low flexural rigidity femoral stems has been associated with higher failure rates [26] and might be a relevant factor for taper mechanics. Smaller diameter necks decrease the stiffness and may elevate fretting subsequent of elastic neck movements within the junction. The finite element modeling showed a tilt of the neck adapter into a permanently inclined position with diagonal contact from lateral-distal to medial-proximal. This nicely corresponds to results of a retrieval study, which found highly worn areas framing local patches on the neck at these locations that presumably led to the failure of those prostheses [11].

Higher assembly forces are likely to increase the initial stability of the taper junction, since less micromotion can occur during load and, therefore, reduce the risk for fretting. This is achieved by deeper seating of the neck adapter as observed in the measurements, which provides increased resistance against permanent neck tilting and motion of the components relative to one another as a result of higher frictional stresses at the interface. Furthermore, small gaps between the components due to unavoidable manufacturing tolerances as well as taper angle differences, might be closed, alleviating the risk of fluid ingress and hence crevice corrosion in-vivo. Assembly forces of around 4000 N are imperative in order to generate a sufficient taper-lock [27]. Measurements in this study showed significantly decreased micromotion (65%) for the prostheses assembled with 4000 N compared with prostheses assembled with 2000 N. That was further supported by FE analyses under condition of assembly with 8000 N, which showed a further reduction of micromotion (95%). These findings are consistent with Haschke et al. [19] who also stated that the assembly force greatly influences the relative motion between neck and stem components in bi-modular hip prostheses [19]. However, excessive assembly forces might put the femur in danger for intraoperative periprosthetic fractures [28], which is an unacceptable risk.

Suspicion has been raised over TMZF as stem material to cause early prosthesis failure following excessive fretting corrosion [12,29]. The FE results show that TMZF exhibited substantially higher micromotion in comparison to conventional Ti6Al4V alloy, which was most prominent for low assembly forces (up to 30%). Lateral gap opening at the proximal taper entrance was also higher in case of TMZF, which potentially facilitates fluid ingress into the junction. The presence of fluid within the taper interface can accelerate the already elevated risk for fretting due to increased micromotion into mechanically assisted crevice corrosion (MACC) as a result of inferior mechanical integrity and stability of the prosthesis due to the lower Young's modulus of the stem (76 GPa vs. 110 GPa).

Interface motions of 5–12 µm have been associated with visible fretting corrosion at the head-stem taper surface after testing [30]. For either stem material investigated in this study, the extent of micromotion assessed at the apexes of the stem-neck junction exceeded these critical values by over six-fold, which emphasises the high susceptibility of the flat taper junction to corrosive processes due to impaired taper mechanics.

This in-vitro study has limitations that are worth mentioning. The testing solely included two specimens, which may not represent the variability between prostheses of this design. The retrieved samples had marginally worn taper surfaces, which might have influenced the micromotion, especially compared to pristine components. Validation of the FE model was confined to the areas of the windows; the determined micromotions outside these regions were numerically projected results. Results for the Ti6Al4V stem were solely generated from FE analyses and were not experimentally validated. However, to the authors' knowledge, so far no micromotion measurements have been acquired in an as close proximity to the real taper contact area between the two parts of a junction as shown in this study.

## 5. Conclusion

Micromotion at the taper junction is influenced by various factors. The present study showed the assembly force as well as the flexural rigidity of the neck and stem to influence the micromotion greatly. A larger assembly force was shown to partly compensate low implant stiffness or larger lever arms. The further the load application from the taper engagement, the higher an assembly force is required. This is confirmed by the high assembly forces applied to modular revision prostheses, which are commonly assembled with forces above 10 kN. Despite the intraoperative variability bi-modular prostheses offer, manufacturers should consider the elevated fretting and corrosion risk during future design processes.

## Declaration statements

### Conflict of interest:

None related to this study

### Ethical approval:

Not required

## Acknowledgments

The research has received funding from the European Union's Seventh Framework Programme (FP7/2007-2013) under grant agreement no. GA-310477 LifeLongJoints.

## References

[1] Banerjee S, Cherian J, Bono J, Kurtz S, Geesink R, Meneghini R, Delanois R, Mont M. Gross trunnion failure after primary total hip arthroplasty. J Arthroplast 2015;30(4):641–8.
[2] Del Balso C, Teeter M, Tan S, Howard J, Lanting B. Trunnionosis: does head size affect fretting and corrosion in total hip arthroplasty? J Arthroplast 2016;31(10):2332–6.
[3] Morlock M, Buente D, Guehrs J, Bishop N. Corrosion of the head-stem taper junction - Are we on the verge of an epidemic? HSS J 2017;13(1):42–9.
[4] Cook R, Bolland B, Wharton J, Tilley S, Latham J, Wood R. Pseudotumour formation due to tribocorrosion at the taper interface of large diameter metal on polymer modular total hip replacements. J Arthroplast 2013;28(8):1430–6.
[5] Stahnke J, Sharpe K. Pseudotumor formation in a metal-on-polyethylene total hip arthroplasty due to trunnionosis at the head-neck taper. Surg Technol Int 2015;27:245–50.
[6] Mann M, Tanzer D, Tanzer M. Severe metal-induced osteolysis many years after unipolar hip endoprosthesis. Clin Orthop Relat Res 2013;471(7):2078–82.

[7] Hallab N, Merritt K, Jacobs J. Metal sensitivity in patients with orthopaedic implants. J Bone Joint Surg Am 2001;83-A(3):428–36.
[8] Graves S, de Steiger R, Davidson D, Donnelly W, Rainbird S, Lorimer M, Cashman K, Vial R. The use of femoral stems with exchangeable necks in primary total hip arthroplasty increases the rate of revision. Bone Joint J 2017;99-B(6):766–73.
[9] Nawabi D, Do H, Ruel A, Lurie B, Elpers M, Wright T, Potter H, Westrich G. Comprehensive analysis of a recalled modular total hip system and recommendations for management. J Bone Joint Surg Am 2016;98(1):40–7.
[10] Bernstein D, Meftah M, Paranilam J, Incavo S. Eighty-six percent failure rate of a modular-neck femoral stem design at 3–5 years: lessons learned. J Bone Joint Surg Am 2016;12(98):e49.
[11] Buente D, Huber G, Bishop N, Morlock M. Quantification of material loss from the neck piece taper junctions of a bimodular primary hip prosthesis. A retrieval study from 27 failed rejuvenate bimodular hip arthroplasties. Bone Joint J 2015;97-B(10):1350–7.
[12] De Martino I, Assini J, Elpers M, Wright T, Westrich G. Corrosion and fretting of a modular hip system: a retrieval analysis of 60 Rejuvenate stems. J Arthroplast 2015;30(8):1470–5.
[13] Meftah M, Haleem A, Burn M, Smith K, Incavo S. Early corrosion-related failure of the rejuvenate modular total hip replacement. J Bone Joint Surg Am 2014;96(6):481–7.
[14] Gilbert J, Buckley C, Jacobs J. In vivo corrosion of modular hip prosthesis components in mixed and similar metal combinations. The effect of crevice, stress, motion, and alloy coupling. J Biomed Mater Res B Appl Biomater 1993;27(12):1533–44.
[15] Goldberg J, Gilbert J, Jacobs J, Bauer T, Paprosky W, Leurgans S. A multicenter retrieval study of the taper interfaces of modular hip prostheses. Clin Orthop Relat Res 2002;401:149–61.
[16] Gilbert J, Mali S, Urban R, Silverton C, Jacobs J. In vivo oxide-induced stress corrosion cracking of Ti-6Al-4V in a neck-stem modular taper: emergent behavior in a new mechanism of in vivo corrosion. J Biomed Mater Res B Appl Biomater 2012;100(2):584–94.
[17] Royhman D, Patel M, Runa M, Wimmer M, Jacobs J, Halleb N, Mathew M. Fretting-corrosion behavior in hip implant modular junctions: the influence of friction energy and pH variation. J Mech Behav Biomed Mater 2016;62:570–87.
[18] Dyrkacz R, Brandt J, Morrison J, O'Brien S, Ojo O, Turgeon T, Wyss U. Finite element analysis of the head–neck taper interface of modular hip prostheses. Tribol Int 2015;91:206–13.
[19] Haschke H, Jauch-Matt S, Sellenschloh K, Huber G, Morlock M. Assembly force and taper angle difference influence the relative motion at the stem-neck interface of bi-modular hip prostheses. Proc Inst Mech Eng H 2016;230(7):690–9.
[20] Derasari A, Gold J, Ismaily S, Noble P, Incavo S. Will new metal heads restore mechanical integrity of corroded trunnions? J Arthroplast 2017;4(32):1356–9.
[21] Buente D, Bryant M, Ward M, Neville A, Morlock M, Huber G. The taper corrosion pattern observed for one bi-modular stem design is related to geometry-determined taper mechanics. Med Eng Phys 2017;46:79–88.
[22] Bergmann G, Deuretzbacher G, Heller M. Hip contact forces and gait patterns from routine activities. J Biomech 2001;34(7):859–71.
[23] Swaminathan V, Gilbert J. Fretting corrosion of CoCrMo and $Ti_6Al_4V$ interfaces. Biomaterials 2012;33(22):5487–503.
[24] Gilbert J, Mehta M, Pinder B. Fretting crevice corrosion of stainless steel stem–CoCr femoral head connections: comparisons of materials, initial moisture, and offset length. J Biomed Mater Res B Appl Biomater 2009;88(1):162–73.
[25] Damm P, Dymke J, Ackermann R, Bender A, Graichen F, Halder A, Beier A, Bergmann G. Friction in total hip joint prosthesis measured in vivo during walking. PLoS One 2013;8(11):e78373.
[26] Wight C, Lanting B, Schemitsch E. Evidence based recommendations for reducing head-neck taper connection fretting corrosion in hip replacement prostheses. Hip Int 2017;27(6):523–31.
[27] Rehmer A, Bishop N, Morlock M. Influence of assembly procedure and material combination on the strength of the taper connection at the head-neck junction of modular hip endoprostheses. Clin Biomech 2012;1(27):77–83.
[28] Lindahl H. Epidemiology of periprosthetic femur fracture around a total hip arthroplasty. Injury 2007;38(6):651–4.
[29] Raju S, Chinnakkannu K, Puttaswamy M, Phillips M. "Trunnion corrosion in metal-on-polyethylene total hip arthroplasty: a case series," vol. 25, no. 2, pp. 133–139, 2017.
[30] Mali SA, Gilbert JL. Correlating fretting corrosion and micromotions in modular Tapers: test method development and assessment. Philadelphia, PA: American Society for Testing and Materials; 2015. ASTM STP 1591 p. 259–82.